

Subcellular dynamics of proteins and metabolites under abiotic stress reveal deferred response of the *Arabidopsis thaliana* hexokinase-1 mutant *gin2-1* to high light

Lisa Küstner^{1,†}, Lisa Fürtauer^{2,†}, Wolfram Weckwerth^{3,4}, Thomas Nägele² and Arnd G. Heyer^{1,*} 

¹Department of Plant Biotechnology, Institute of Biomaterials and Biomolecular Systems, University of Stuttgart, Pfaffenwaldring 57, 70569 Stuttgart, Germany,

²Department Biology I, Plant Evolutionary Cell Biology, Ludwig-Maximilians-University Munich, Großhaderner Str. 2-4, 82152 Planegg-Martinsried, Germany,

³Department of Ecogenomics and Systems Biology, University of Vienna, Althanstraße 14, 1090 Vienna, Austria, and

⁴Vienna Metabolomics Center, University of Vienna, Althanstraße 14, 1090 Vienna, Austria

Received 25 February 2019; revised 22 July 2019; accepted 29 July 2019; published online 6 August 2019.

*For correspondence (e-mail arnd.heyer@bio.uni-stuttgart.de).

†These authors contributed equally to this work.

SUMMARY

Stress responses in plants imply spatio-temporal changes in enzymes and metabolites, including subcellular compartment-specific re-allocation processes triggered by sudden changes in environmental parameters. To investigate interactions of primary metabolism with abiotic stress, the *gin2-1* mutant, defective in the sugar sensor hexokinase 1 (HXK1) was compared with its wildtype *Landsberg erecta* (*Ler*) based on time resolved, compartment-specific metabolome and proteome data obtained over a full diurnal cycle. The high light sensitive *gin2-1* mutant was substantially delayed in subcellular re-distribution of metabolites upon stress, and this correlated with a massive reduction in proteins belonging to the ATP producing electron transport chain under high light, while fewer changes occurred in the cold. In the wildtype, compounds specifically protecting individual compartments could be identified, e.g., maltose and raffinose in plastids, myo-inositol in mitochondria, but *gin2-1* failed to recruit these substances to the respective compartments, or responded only slowly to high irradiance. No such delay was obtained in the cold. At the whole cell level, concentrations of the amino acids, glycine and serine, provided strong evidence for an important role of the photorespiratory pathway during stress exposure, and different subcellular allocation of serine may contribute to the slow growth of the *gin2-1* mutant under high irradiance.

Keywords: *Arabidopsis thaliana*, stress response, subcellular compartmentation, hexokinase 1, *gin2-1*, high light treatment, cold treatment.

INTRODUCTION

Due to their sessile lifestyle, plants are exposed to rapidly changing environmental conditions, like sudden oscillations in light intensity or a fast drop of temperature, and restoration of a physiological homeostasis requires massive subcellular reprogramming of metabolism (Nägele and Heyer, 2013; Hoermiller *et al.*, 2017). Because most abiotic stresses will inevitably result in the production of reactive oxygen species (ROS; Mittler, 2002; Foyer and Noctor, 2003; You and Chan, 2015; Choudhury *et al.*, 2017), monitoring the redox balance of individual cellular compartments can trace the challenge caused by abiotic stress at high spatio-temporal resolution. Besides being toxic byproducts of aerobic metabolism, ROS also play an

important role as signalling molecules during stresses, such as wounding and pathogen attack, or for the acclimation to high light and cold (Bolwell and Wojtaszek, 1997; Foyer *et al.*, 1997; Alvarez *et al.*, 1998; Karpinski, 1999; Baxter *et al.*, 2014; Foyer and Noctor, 2015; Mittler, 2017). Another class of signalling molecules reporting on cellular homeostasis are soluble sugars and sugar phosphates that inform the cell about its carbon and energy status and guide metabolic reprogramming and growth (Smeekens *et al.*, 2010). The enzyme hexokinase (HXK1) was identified as a glucose sensor that establishes a link between primary metabolism and hormonal regulation, and the *gin2-1* mutant of *Arabidopsis*, defective in HXK1, shows reduced

growth and delayed flowering and senescence (Moore *et al.*, 2003). The *gin2-1* allele of HXK1 comprises a non-sense mutation (Q432*) and is therefore defective in its hexose phosphorylation activity as well as the sugar sensing function, the detailed mechanism of which is still not fully understood (Cho *et al.*, 2006). Nevertheless, it is clear that sugar sensing and signalling is pivotal for modulating not only growth and development, but also stress responses (Harrington and Bush, 2003; Cho *et al.*, 2006; Rolland *et al.*, 2006; Yu *et al.*, 2013). The *gin2-1* mutant is known to be high light sensitive and displays increasing growth retardation at rising light intensities (Moore *et al.*, 2003). The cause for high light sensitivity of *gin2-1* is not clear, although it is unlikely to be due to a general deficiency in carbon metabolism (Moore *et al.*, 2003). As a kinase phosphorylating hexoses, HXK1 is involved in the so-called sucrose cycle, the hydrolysis of sucrose by invertases and its subsequent re-synthesis from fructose-6-phosphate and UDP-glucose via the enzyme sucrose-phosphate synthase (Huber, 1989). This cycle, which can contribute about one quarter of sucrose synthesis, plays an important role in stabilizing the cellular sucrose concentration (Nägele *et al.*, 2010). Because sucrose functions as long-distance transport form of reduced carbon, a loss of HXK1 results in elevated sucrose export from leaves (Brauner *et al.*, 2015). Under abiotic stresses, e.g., low temperatures, sucrose is accumulated and also serves as substrate for the synthesis of the trisaccharide raffinose, which has a protective function for photosystem II (Knaupp *et al.*, 2011). A reduction in sucrose cycling may therefore interfere with restoration of metabolic homeostasis under changing environmental conditions.

Most studies analyzing plant stress responses used whole cell extracts, thus yielding an average of metabolite concentrations in the various compartments of a plant cell. This may lead to misinterpretations, given the large differences in relative size of subcellular structures, e.g., central vacuole as compared to plastids, and also the allocation of metabolites to individual compartments. Thus, understanding responses of plants to abiotic stress affords analysis of subcellular distribution of metabolites as well as their re-allocation during stress exposure (Foyer and Noctor, 2015; Jorge *et al.*, 2016). Subcellular re-distribution under different light conditions of small molecules associated with redox balance, e.g., ascorbate, glutathione and H₂O₂, has been achieved using different cytochemical labelling techniques (Blokhina, 2001; Orozco-Cárdenas *et al.*, 2001; Zechmann, 2011; Heyneke *et al.*, 2013). However, a full picture of metabolic homeostasis at subcellular resolution is lacking. A useful tool to study subcellular compartmentation of many metabolites in parallel is the non-aqueous fractionation (NAF) of freeze-dried plant material. As an example, this method was used to show an important role of raffinose in plastids, but not the cytosol,

at low temperatures (Schneider and Keller, 2009; Knaupp *et al.*, 2011; Nägele and Heyer, 2013; Fürtauer *et al.*, 2016; Hoermiller *et al.*, 2017). Additional techniques and applications for different stress conditions are reviewed in Jorge *et al.* (2016) and Dietz (2017).

Here and in an accompanying article (Fürtauer *et al.*, 2019), this technique was employed for a spatiotemporally resolved metabolomics and proteomics study of plant stress responses. In the current study, two different abiotic stress conditions, high light (1200 $\mu\text{mol m}^{-2} \text{sec}^{-1}$, max. 30°C) and low temperature (120 $\mu\text{mol m}^{-2} \text{sec}^{-1}$, 1°C), were applied to the *gin2-1* mutant and its respective wild-type, the accession Landsberg erecta (*Ler*), to investigate how hexokinase contributes to stress responses of photosynthetically active plant cells.

RESULTS

Subcellular redox states differ among compartments and time points

In a first step towards spatial resolution of cellular redox balance, transgenic plants expressing the reduction–oxidation-sensitive green fluorescence protein 2 (roGFP2) were used to investigate subcellular reduction states under the experimental conditions used in this study. Transgenic lines in the Col-0 background expressing roGFP2 either in the mitochondria, chloroplasts, peroxisomes or cytosol were exposed to high light conditions. Significant treatment effects on the degree of oxidation (OxD) were observed for all compartments; however, at different time points (Figure 1a–d). While chloroplasts and peroxisomes responded quickly, mitochondria and cytosol showed a high light effect only after 10 h. Interestingly, at that time point, symptoms had already disappeared in the chloroplasts, while all other compartments showed higher degrees of oxidation together with enhanced reduction potentials (Figure 1). This suggests that high light treatment affected chloroplasts at least transiently, thus probably influencing photosynthesis and C-fixation especially in the first hours of stress treatment. C-fixation and allocation were shown to be altered in the hexokinase 1 deficient mutant *gin2-1* (Küstner *et al.*, 2019) under high light exposure. For a detailed analysis of high light effects on primary metabolism, *gin2-1* was chosen to unravel changes in subcellular metabolic reprogramming upon high light and cold stress. The *gin2-1* mutant was created in the genetic background of *Ler*. *Ler* and Col-0 are close relatives (Houshyani *et al.*, 2012), thus allowing to assume that high light effects on subcellular redox state might be similar in both accessions.

The *gin2-1* mutant has elevated heat dissipation and reduced C-fixation under high light

Chlorophyll fluorescence measurements revealed significant differences during the light phase between *Ler* and

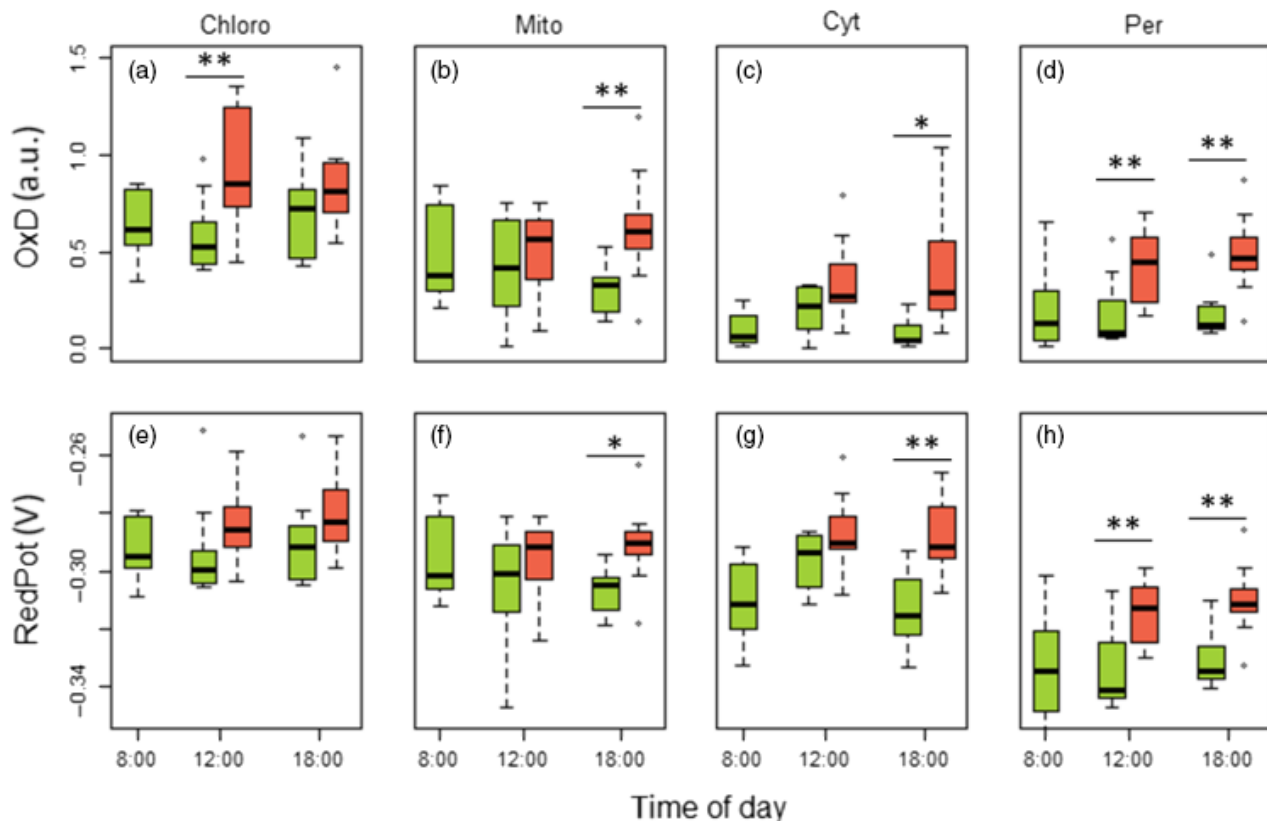


Figure 1. Box-and-whiskers plot of the degree of oxidation (OxD, arbitrary units; a–d) and reduction potential (RedPot, Volt; e–h) of roGFP2 lines for different compartments. Light was turned on at 08:00, samples were measured under control (green) and high light (red) conditions after 4 and 10 h in light ($n = 12$). (a, e) Chloroplasts (Chloro); (b, f) mitochondrion (Mito); (c, g) cytosol (Cyt); and (d, h) peroxisomes (Per). * $P < 0.05$; ** $P < 0.005$ (two-sided Student's *t*-test for treatment).

gin2-1 especially under high light (Figure 2 and Table S1): While F_v/F_m and non-photochemical quenching (NPQ) (Figure 2a,b) were both lower in *Ler* under high light ($P < 0.01$), qP ($P < 0.03$) and qY ($P < 0.004$) were higher (Figure 2c,d). F_v/F_m is a very robust and widely used parameter indicating integrity of photosystem (PS) II (Björkman and Demmig, 1987). Here, mean values (\pm SEM) of 0.775 ± 0.004 for *gin2-1* and 0.756 ± 0.006 for *Ler* under high light condition were found. Values for NPQ during the light phase were significantly higher in *gin2-1* under control and high light, indicating that *gin2-1* dissipated more light energy as heat. Accordingly, photochemical quenching (qP) and yield (qY) were significantly lower in *gin2-1* during the light phase, indicating a higher rate of carbon fixation in *Ler* under high light. Although these differences appear small at increasing photon flux intensity, the persistence over the entire light phase points to their contribution to the growth difference between the two genotypes.

Stress treatment separates primary metabolome and proteome of both genotypes

The primary metabolome was resolved in *Ler* and *gin2-1* for both treatments and all time points. Based on a

principal component analysis (PCA) of the combined data sets of *Ler* and *gin2-1*, the three conditions (control, high light and cold) clearly differed from each other (Figure 3a). Component 1 explained ~34% of variance, and separated the high light condition from cold and control. Component 2 (~16% variance explained) revealed a separation of cold and control treatment with high light samples being located in between. Although it was not possible to conspicuously identify whole metabolic pathways discriminating the treatments, certain metabolites with strong effects on separation could be identified. For the cold treatment, these were citrate and gluconic acid as well as hexoses, while for the high light treatment branched-chain amino acids, glycine as well as proline and, to a lesser extent, raffinose separated the conditions (Figure 3a). Separation of the genotypes is visible under control condition, although not as clear as for the high light and cold treated plants. Separation of *Ler* and *gin2-1* is based on several amino acids, e.g., threonine, serine, glutamate and tyrosine and on the carbonic acids citrate, succinate, gluconate and threonate. After 10 h high light treatment, a distinction of the genotypes was expected because of the high light sensitivity of *gin2-1*. This separation could be traced back to

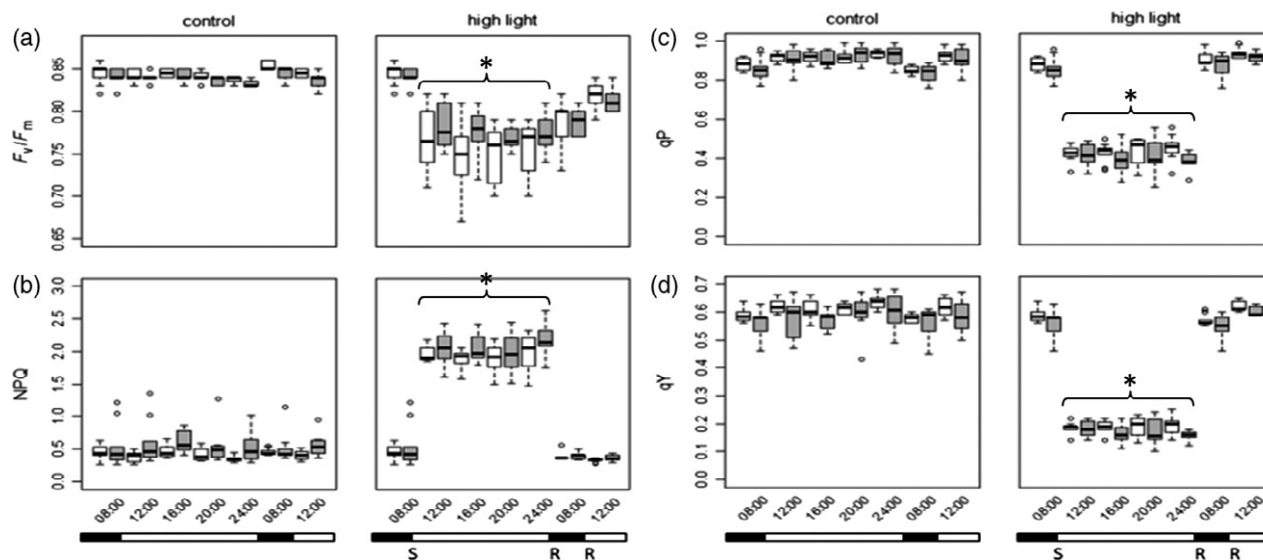


Figure 2. Box-and-whiskers plots of diurnal chlorophyll fluorescence measurements. (a) F_v/F_m ; (b) NPQ (non-photochemical quenching); (c) pQ (photochemical quenching); (d) pY (PSII quantum yield) for *Ler* (white) and *gin2-1* (grey) under control (left panels) or high light (right panels) conditions ($n \geq 7$). Dark/light cycles are indicated as white and black bars below the time line. Stress application is indicated by 'S' with subsequent recovery 'R' in dark and normal light conditions. Significant differences during the light phase (8:00–24:00) between *Ler* and *gin2-1* were identified by ANOVA for genotype and are marked with a * ($P < 0.05$).

proline, fructose, raffinose, the organic acids and oxaloacetate (Figure 3c). After 10 h cold treatment, separation of genotypes arose from the polyamine putrescine and several organic acids, e.g. succinate, fumarate, gluconate and citrate (Figure 3d). PCA after 4 h of stress likewise demonstrated separation of genotypes (Figure S1).

High light caused accumulation of several metabolites in both genotypes (Table 1): (i) tyrosin and branched-chain amino acids isoleucine, leucine and valine, which are precursors for the production of secondary metabolites; (ii) sugars like glucose, fructose, sucrose and raffinose, accumulation of which may result from higher photosynthetic activity; and (iii) glycine, being a product of photorespiration (Foyer *et al.*, 2009; Sicher and Barnaby, 2012). Protein abundance revealed distinct responses of both genotypes under stress. *Ler* displayed a stronger reduction of protein abundance when shifted to low temperature, while *gin2-1* had more proteins reduced in high light (Figure 4). In *gin2-1*, the total number of proteins being less abundant exceeded that of proteins accumulating under high light conditions at both time points, while this was not the case after 10 h in *Ler*. Interestingly, after a 10 h cold treatment, both genotypes had more proteins with increased than with reduced abundance, pointing to an onset of metabolic adjustment. At the initial hours of stress treatment, the impact of high light on protein abundance in *gin2-1* was greater than for cold. About 580 proteins were less abundant under high light, but only 86 were enriched in *gin2-1*. While only nine proteins were enriched in both genotypes under 4 h high light, the number of commonly reduced proteins was 153 (Figure 4).

Assignment and categorization of proteins with significantly different abundance (t-test, $P < 0.05$) using the

MapMan tool (Thimm *et al.*, 2004) yielded an overview of affected metabolic pathways (Figure S2). Both genotypes showed higher dynamics of proteins within the first 4 h compared with 10 h of stress conditions. However, in the category 'light reactions', and here particularly for proteins belonging to the family of light harvesting complex I and II (LHCI and LHCII) as well as polypeptide subunits of Photosystem I (PSI) and PSII, were higher abundant in *Ler* compared to *gin2-1* for both time points (Figures S2a,b and S4a,b). After 4 h high light, proteins related to amino acid biosynthesis and, after 10 h, tricarboxylic acid (TCA) cycle enzymes showed higher abundance in *Ler* than *gin2-1* (Figure S2a,b). For both genotypes, a much larger number of proteins changed abundance after 4 h (358 *Ler* cold, 480 *Ler* high light (HL), 272 *gin2-1* cold, 665 *gin2-1* HL) than after 10 h (33 *Ler* cold, 62 *Ler* HL, 112 *gin2-1* cold, 104 *gin2-1* HL), indicating formation of a new homeostasis. Especially for the 'light reactions', this seemed more successful in *Ler* as compared with *gin2-1* (Figure S2c–f).

Cold treatment caused strong distinction of genotypes regarding metabolites. Yet, fewer differences were found for protein abundance (Figure S3a,b). Compared to control condition, both genotypes showed reduced protein abundance after 4 h in the cold (*Ler*: 315 reduced, 43 increased, *gin2-1*: 243 reduced, 29 increased) for almost all categories (Figure S3c,e). However, after 10 h the protein abundance rose in *gin2-1* (*gin2-1*: 3 reduced, 109 increased, *Ler*: 5 reduced, 28 increased), most evidently for proteins belonging to amino acid biosynthesis and degradation as well as to sugar and starch metabolism (Figure S3f).

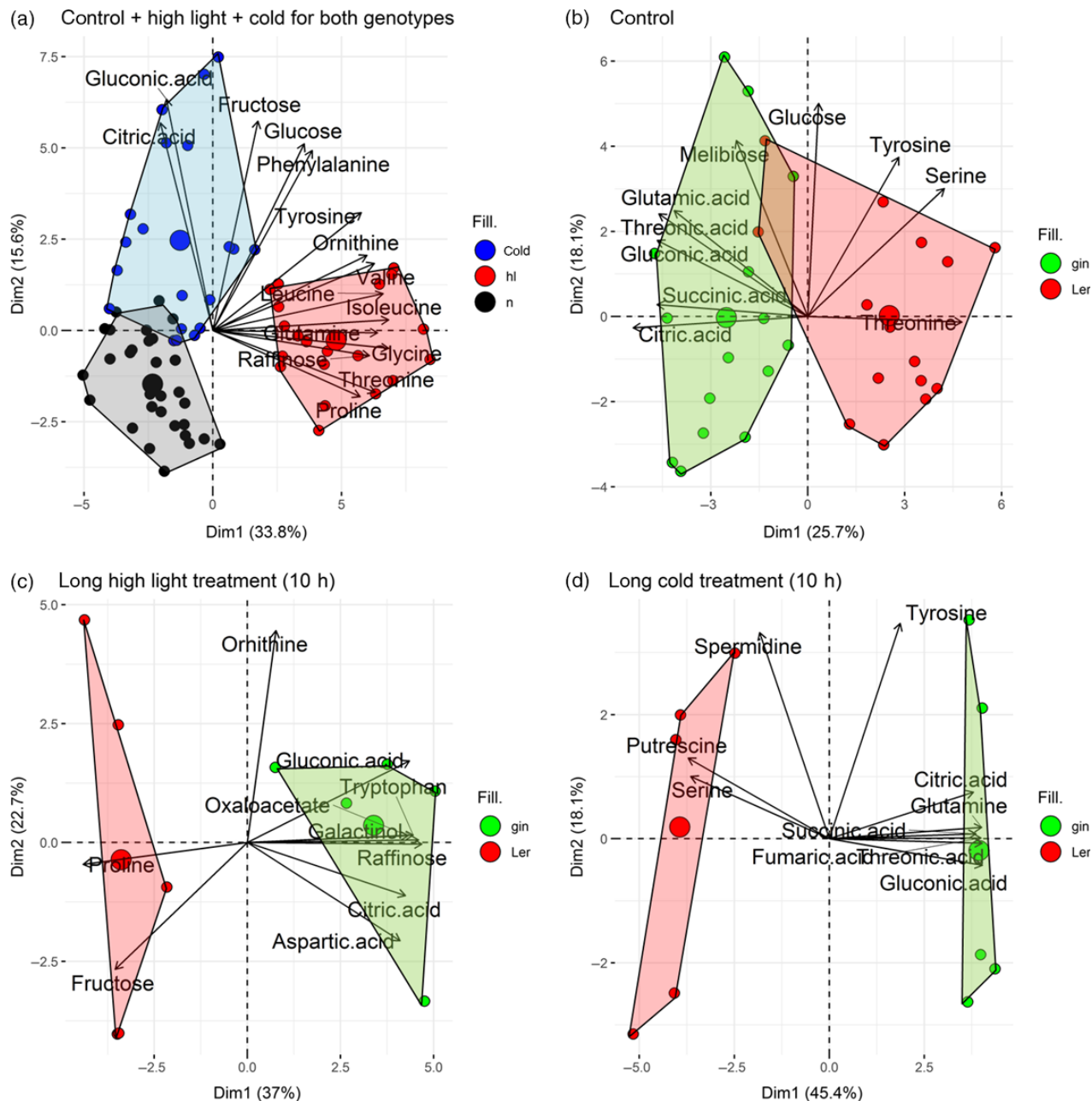


Figure 3. Principal component analysis (PCA). (a) z-Normalized primary metabolite concentrations for control (grey), high light (red) and cold (blue) treatment. All considered genotypes and time points were included ($n \geq 20$). (b) PCA of primary metabolites under the control condition ($n = 15$) for *Ler* (red) and *gin2-1* (green). (c) PCA of primary metabolites after 10 h high light exposure. (d) PCA of primary metabolites after 10 h cold exposure; red: *Ler* ($n = 5$), green: *gin2-1* ($n = 5$). Most contributing metabolites for separation are shown. Small dots represent means of all determined metabolites per genotype and time point; large dots represent means of all metabolites and all individuals of the specified group.

Metabolite association with chloroplasts

Subcellularly resolved metabolome analysis identified several metabolites differentially associating with the chloroplasts at distinct time points and environmental conditions in each of the genotypes (Table 2). The major difference in the response of both lines to either stress condition was a slower translocation to (e.g.,

proline, serine) or delayed retention of several metabolites within chloroplasts in the *gin2-1* mutant. These are high-lighted in Table 2 and shown in the Figures 5 and 6, where a significant difference for proline and serine distribution between *Ler* and *gin2-1* for the plastids after 4 h HL stress can be found (t-test, $P < 0.05$).

Table 1 Metabolite concentrations (means \pm SD, $n = 5$) at whole cell level (nmol g^{-1} DW) for control (N) and high light (HL) treated plants. Statistical differences between the control and its respective high light condition (for example 4 h N Ler ~4 h HL Ler) are marked with an * (Student's t-test, $P < 0.05$)

	Tyrosine	Isoleucine	Leucine
0hN_Ler	39.3 \pm 8.6	193.6 \pm 45.9	110.2 \pm 35.1
4hN_Ler	47.9 \pm 22.5	168.4 \pm 60.0	105.7 \pm 33.8
10hN_Ler	60.3 \pm 22.3	168.7 \pm 61.6	131.6 \pm 54.5
4hHL_Ler	114.7* \pm 51.5	425.2* \pm 168.2	274.8* \pm 89.8
10hHL_Ler	135.4 \pm 77.7	386.1* \pm 201.6	271.9 \pm 163.6
0hN_gin2-1	40.5 \pm 32.0	102.7 \pm 46.7	89.9 \pm 58.7
4hN_gin2-1	37.6 \pm 16.6	96.0 \pm 37.3	51.3 \pm 27.0
10hN_gin2-1	60.0 \pm 35.6	158.8 \pm 59.5	110.6 \pm 47.0
10hHL_gin2-1	108.2* \pm 99.4	342.1* \pm 121.1	189.0* \pm 63.4
10hHL_gin2-1	143.8* \pm 54.9	500.3* \pm 229.9	248.1 \pm 119.4
	Valine	Glycine	Glucose
0hN_Ler	1593.1 \pm 496.6	362.1 \pm 934.6	6257.3 \pm 344.4
4hN_Ler	866.2 \pm 285.9	936.0 \pm 14 529.2	17 276.3 \pm 8171.3
10hN_Ler	1300.5 \pm 449.3	1939.8 \pm 3659.8	9632.6 \pm 1304.4
4hHL_Ler	2161.5* \pm 1259.1	42 601.1* \pm 14 176.6	42 991.4* \pm 13 394.7
10hHL_Ler	2573.8* \pm 798.0	67 842.4* \pm 17 390.7	23 035.3 \pm 14 167.5
0hN_gin2-1	805.6 \pm 165.1	179.2 \pm 1341.8	2827.1 \pm 441.4
4hN_gin2-1	838.6 \pm 126.4	596.3 \pm 3793.4	8527.1 \pm 2333.2
10hN_gin2-1	919.4 \pm 250.7	924.6 \pm 6680.4	9257.4 \pm 1934.6
4hHL_gin2-1	1926.4* \pm 181.6	37 145.7* \pm 6538.1	25 247.4* \pm 7977.7
10hHL_gin2-1	2740.7* \pm 818.7	68 701.4* \pm 5404.0	14 518.6 \pm 823.5
	Fructose	Sucrose	Raffinose
0hN_Ler	3024.5 \pm 6410.0	25 215.5 \pm 525.9	611.7 \pm 217.7
4hN_Ler	9959.0 \pm 6859.3	30 222.5 \pm 933.1	991.5 \pm 284.6
10hN_Ler	4913.5 \pm 3344.5	21 525.2 \pm 422.2	742.6 \pm 414.6
4hHL_Ler	36 273.2* \pm 11 053.2	47 001.6* \pm 1211.3	2577.2* \pm 17 495.1
10hHL_Ler	8417.8 \pm 5753.4	35 328.4* \pm 1263.4	1545.8 \pm 16 471.6
0hN_gin2-1	847.6 \pm 4966.2	17 605.4 \pm 530.1	240.9 \pm 154.7
4hN_gin2-1	2962.1 \pm 2398.4	22 480.1 \pm 494.0	340.6 \pm 178.7
10hN_gin2-1	2619.6 \pm 4552.9	18 318.4 \pm 492.3	831.2 \pm 270.3
4hHL_gin2-1	10 931.8* \pm 5223.1	34 976.5* \pm 1250.0	2313.5* \pm 12 135.6
10hHL_gin2-1	2335.4 \pm 3908.9	27 870.0* \pm 1433.1	4506.2* \pm 21 430.6

Metabolites supposed to have protective functions were associated with chloroplasts already after 4 h of treatment in *Ler*, but not in *gin2-1*. Some of these metabolites became associated with chloroplasts of *gin2-1* after 10 h, but some failed completely. Proline, serine and threonine associated with the chloroplasts in *gin2-1* only after 10 h of exposition to HL, but already after 4 h in *Ler*. Maltose, tryptophan and alanine were not at all associated with chloroplasts in *gin2-1* under HL. In cold, only proline and serine behaved similar to the HL treatment. Not only the speed but also the degree of plastidial association of proline and serine differed between *Ler* and *gin2-1*. Total proline and total serine content on a whole cell basis were also higher in *Ler* than *gin2-1*. At the subcellular level, *Ler* had roughly 65–80% of its proline associated with the chloroplasts following a 4 h cold or HL treatment. Chloroplasts of *gin2-1*, however, contained only 55% of proline in the cold and

40% after 4 h HL treatment, the latter being significantly lower ($P < 0.05$) as compared to *Ler*. Even after 10 h of HL, plastidial proline content in *gin2-1* did not exceed 65% (Figure 5).

A similar pattern was observed for serine. *Ler* contained more serine under control conditions, but under HL both genotypes showed similar levels. The subcellular distribution to some extent reflected that of proline with 55 and 75% plastidial localization after 4 and 10 h, respectively, in both genotypes under control conditions. Under HL, however, 65% of serine was re-distributed to the chloroplasts in *Ler* after 4 and 10 h, while in *gin2-1* 30 and 60% serine became plastidial after 4 and 10 h, respectively (Figure 6). Again, the plastidial fraction after 4 h HL treatment was significantly lower in *gin2-1* as compared to *Ler*.

Maltose, tryptophan and alanine were associated with the chloroplasts only in HL treated *Ler* but not *gin2-1*.

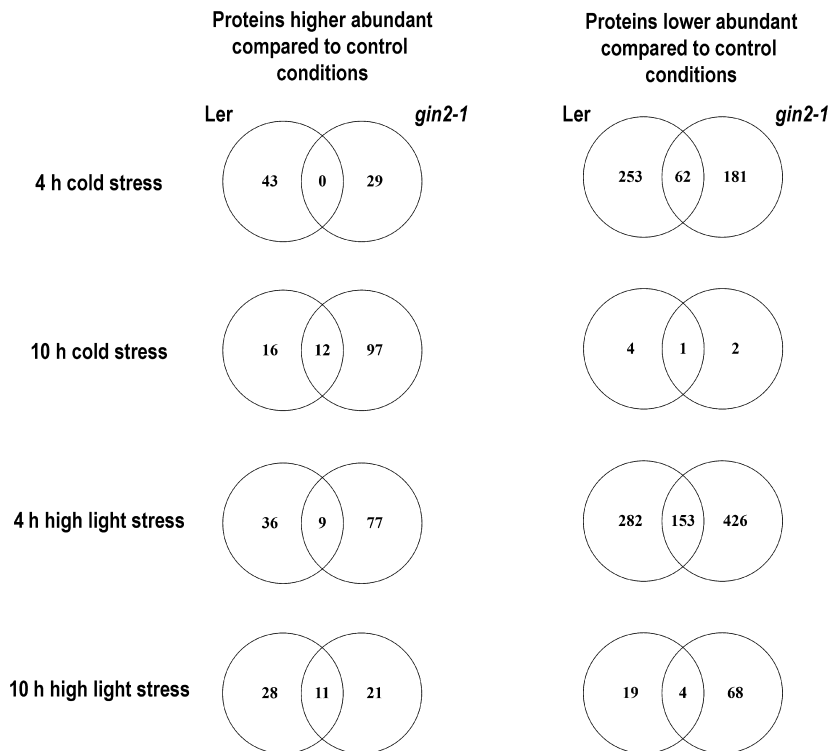


Figure 4. Venn diagrams of proteins with higher and lower abundance after 4 and 10 h stress treatment compared with respective control conditions in *Ler* (left side) and *gin2-1* (right side). (High-light: $n \geq 3$, cold: $n = 3$. Student's t-test comparing treatment vs. control, $P < 0.025$, Bonferroni corrected.)

Presently, evidence supporting a protective role for alanine is lacking, while a destabilizing effect of tryptophan was shown for thylakoid membranes *in vitro* (Popova *et al.*, 2002). However, maltose was assigned a function as substrate for sucrose synthesis at least in the cold (Sicher, 2011), possibly explaining the large rise of maltose in the cold condition. Although *gin2-1* seemed to have a more prominent rise in whole cell maltose concentration under the cold condition, there was no significant difference between the two genotypes regarding the plastidial share. However, under HL, 60% of maltose were found to be associated with plastids in *Ler* after 4 h, but much less (t-test, $P < 0.05$), i.e. only 20%, of the maltose were associated with plastids in *gin2-1*. After 10 h treatment both genotypes had roughly 55–60% of their maltose associated with the plastids (Figure 7).

Metabolites associated with mitochondria

Combining NAF with extensive protein analysis allowed for discrimination of mitochondria from other subcellular compartments (Fürtauer *et al.*, 2019) and thus, some metabolites could be assigned to this organelle. Citrate, for example, was assigned to the mitochondria in the four-compartment-model, while it appeared plastidial in the three-compartment-model (Fürtauer *et al.*, 2019). In some cases, mitochondrial assignment was difficult to interpret. For example, attribution of a large proportion of sucrose to the mitochondria was repeatedly obtained. As discussed in the accompanying paper (Fürtauer *et al.*, 2019), the four-

compartment-model appears to prevent overestimation of plastidial metabolite proportions, but may underestimate plastid localized metabolites, e.g. sugars. Nevertheless, association of proline, serine and, additionally, of sucrose and myo-inositol with the mitochondria was faster in *Ler* (after 4 h) as compared with *gin2-1* (after 10 h) in HL, as already shown for the plastidial compartment. No such effects were found in cold treated plants. In contrast, galactinol and maltose seemed to associate stronger with mitochondria in *gin2-1* than in *Ler*. Considering that diffusion of galactinol into cellular organelles has been described for *Ajuga reptans* and spinach (Schneider and Keller, 2009), association with non-cytosolic compartments may indicate reduced turnover by the cytosolic raffinose synthase, which is in accordance with a lower raffinose content in cold-treated *gin2-1* (see Figure 8). Association of spermidine with the mitochondria under HL was lost after 10 h in *gin2-1* but not in *Ler* (Table 3). Spermidine is known to have protective functions against oxidative damage (Minocha *et al.*, 2014). The loss of association of spermidine with the mitochondria in *gin2-1* after 10 h HL treatment may thus contribute to the HL sensitivity of this genotype.

DISCUSSION

Compartment-specific responses to HL stress

The strong compartmentation of plant metabolism is a key issue impeding investigation and understanding of metabolic changes in plant leaves in response to abiotic stress

Table 2 Metabolite association with chloroplasts for *Ler* (L) and *gin2-1* (G) under high light (red) and cold stress conditions (blue). (x): significant ($P < 0.05$) correlation of metabolite distribution and chloroplast marker protein distribution (Pearson's r); (n.d.): not detected. Highlighted are those metabolites that are either only associated with chloroplasts of *Ler* or later associated with the chloroplasts in *gin2-1* (10 h exposition)

	Control						Cold				High light			
	0 h		4 h		10 h		4 h		10 h		4 h		10 h	
	L	G	L	G	L	G	L	G	L	G	L	G	L	G
2-Oxoglutarate	n.d.	n.d.	n.d.	n.d.	n.d.	n.d.								x
Alanine	x				x	x	x			x			x	x
Asparagine					x				x	x				x
Aspartic acid	x	x	x	x	x	x	x	x	x	x	x	x	x	x
Citric acid									x					x
Fructose														
Fumaric acid														
Galactinol	x	x			x		x	x		x		x	x	x
Gluconic acid														
Glucose														
Glutamic acid	x	x	x	x			x	x	x	x	x	x		x
Glutamine	x	x	x	x					x	x	x	x		
Glycine														
Isoleucine					x		x		x		x			
Leucine					x		x		x		x			
Lysine		x	x	x							x			
Malic acid													x	x
Melibiose														
Methionine	x	x	x	x	x	x	x	x	x	x	x	x		
Ornithine	x	x			x	x	x	x	x	x	x	x	x	x
Oxaloacetate	n.d.	n.d.	n.d.	n.d.	n.d.	n.d.								n.d.
Phenylalanine	x		x		x	x	x	x	x	x				
Proline					x		x	x	x	x	x	x	x	x
Putrescine	x	x	x	x	x	x	x	x	x	x	x	x		x
Pyruvic acid													x	
Raffinose													x	x
Serine			x	x			x	x	x	x	x	x	x	x
Spermidine	x	x	x	x									x	x
Succinic acid														x
Sucrose					x		x		x		x	x	x	x
Threitol														
Threonic acid	x	x	x	x	x	x	x	x	x	x	x	x	x	x
Threonine		x			x		x		x		x		x	x
Tryptophan	x	x	x	x			x		x		x		x	
Tyrosine		x	x				x							
Valine					x		x		x					
myo-Inositol	x	x	x	x	x	x	x	x	x	x	x	x	x	x
Maltose	x	x			x		x	x	x	x	x	x	x	

(Noctor *et al.*, 2015; Jorge *et al.*, 2016). This and the accompanying study (Fürtauer *et al.*, 2019) seek to address this problem by combining compartment-specific primary metabolome and proteome analysis of plant leaves exposed to abiotic stress. The redox-sensitive roGFP2 probe demonstrated that HL stress affected the cellular redox balance in a compartment-specific manner (Figure 1). Chloroplasts showed an elevated OxD already 4 h after onset of high irradiance (Figure 1a), while this transduced to the cytosol and mitochondria only after 10 h of stress exposure (Figure 1b,c). At that time, plastids had

already re-established a redox homeostasis, while a higher OxD persisted in peroxisomes over the entire HL treatment (Figure 1d). This, most likely, reflects elevated photorespiratory activity, which is supported by a rapid increase in glycine levels under high irradiance (Figure 3a). Interestingly, elevation of OxD in mitochondria was delayed. Raghavendra *et al.* (1998) have suggested redox exchange between peroxisomes and mitochondria via oxaloacetate and malate to provide NADH for reduction of hydroxypyruvate in peroxisomes. They showed that metabolite exchange between the two compartments took 90 min to

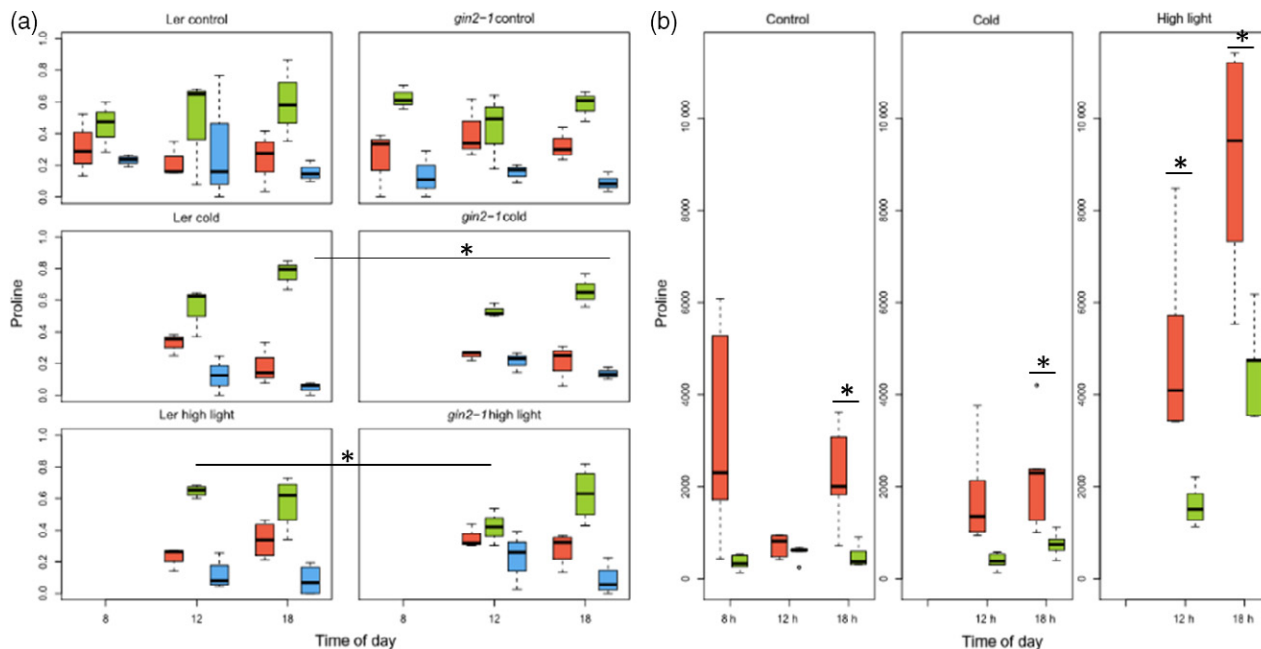


Figure 5. Box-and-whisker plots of (a) subcellular distributions (in %; $n = 3$; red: cytosol, green: plastid, blue: vacuole) using the three compartment model; and (b) whole cell concentrations (nmol gDW^{-1} ; $n = 5$; red: *Ler*, green: *gin2-1*) of proline for control, high light or cold exposition. Significant changes between *Ler* and *gin2-1* for a given time point–treatment combination either for a specific compartment (a) or on the whole cell basis (b) are marked by * (two-sided t-test, $P < 0.05$).

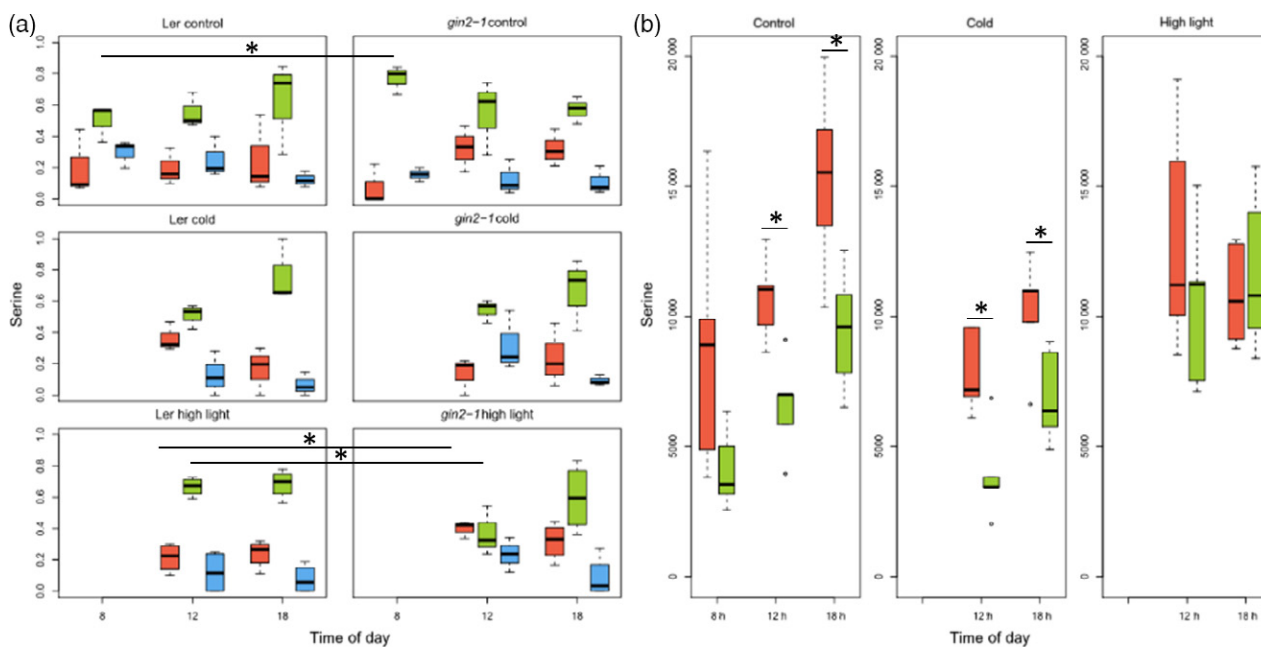


Figure 6. Box-and-whisker plots of (a) the subcellular distributions (in %; $n = 3$; red: cytosol, green: plastid, blue: vacuole) using the three compartment model; and (b) whole cell concentrations (nmol gDW^{-1} ; $n = 5$; red: *Ler*, green: *gin2-1*) of serine for control, high light or cold exposition. Significant changes between *Ler* and *gin2-1* for a given time point–treatment combination either for a specific compartment (a) or on the whole cell basis (b) are marked by * (two-sided t-test, $P < 0.05$).

reach half of its maximal rate, thus indicating that redox transfer between peroxisomes and mitochondria has a substantial time lag.

As an independent measure of HL stress in plastids, ChlF was recorded for the genotypes *Ler* and *gin2-1*, the latter being known for its HL sensitivity (Moore *et al.*, 2003). This

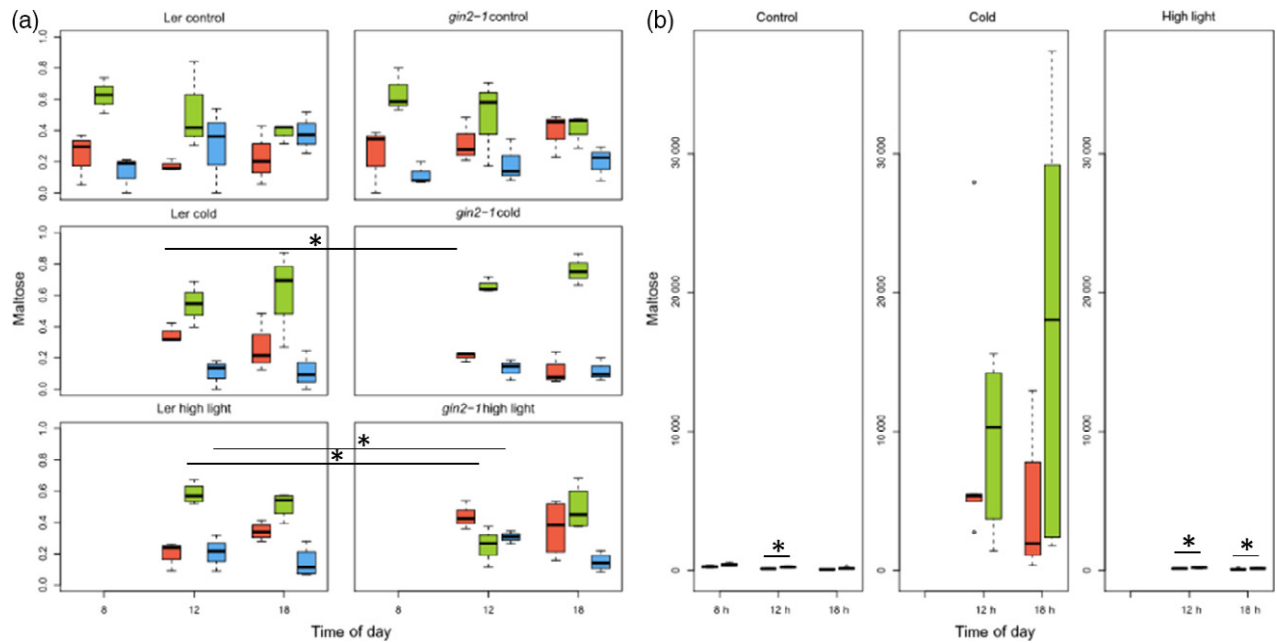


Figure 7. Box-and-whisker plots of (a) the subcellular distributions (in %; $n = 3$; red: cytosol, green: plastid, blue: vacuole) using the three compartment model and (b) whole cell concentrations (nmol gDW⁻¹; $n = 5$; red: *Ler*, green: *gin2-1*) of maltose for control, high light or cold exposition. Significant changes between *Ler* and *gin2-1* for a given time point–treatment combination either for a specific compartment (a) or on the whole cell basis (b) are marked by * (two-sided t-test, $P < 0.05$).

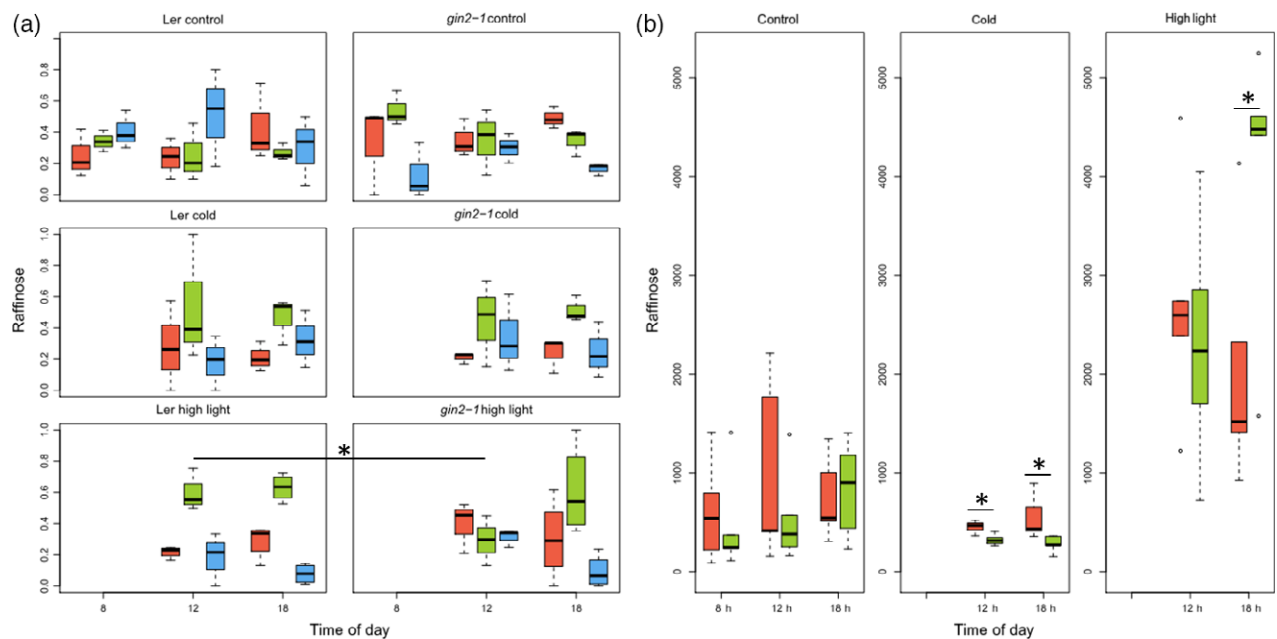


Figure 8. Box-and-whisker plots of (a) the subcellular distributions (in %; $n = 3$; red: cytosol, green: plastid, blue: vacuole) using the three compartment model and (b) whole cell concentrations (nmol g⁻¹ DW; $n = 5$; red: *Ler*, green: *gin2-1*) of raffinose for control, high light or cold exposition. Significant changes between *Ler* and *gin2-1* for a given time point–treatment combination either for a specific compartment (a) or on the whole cell basis (b) are marked by * (two-sided t-test, $P < 0.05$).

revealed a fast and persisting reduction of maximum quantum yield and photochemical quenching, while NPQ was strongly increased. Considering robustness of the F_v/F_m

parameter, the significantly lower reduction under HL in *gin2-1* as compared to *Ler* (Figure 2a) indicates different responses to high irradiance in the two genotypes. There

Table 3 Metabolite association with mitochondria for *Ler* (L) and *gin2-1* (G) under high light (orange) and cold stress conditions (blue). (x): significant ($P < 0.05$) correlation of metabolite distribution and mitochondrial marker protein distribution (Pearson's r); (n.d.): not detected. High lighted are those metabolites that are either only associated with mitochondria of *Ler* or later associated with the mitochondria in *gin2-1* (10 h exposition)

	Control						Cold				High light			
	0 h		4 h		10 h		4 h		10 h		4 h		10 h	
	L	G	L	G	L	G	L	G	L	G	L	G	L	G
2-Oxoglutarate	n.d.	n.d.	n.d.	n.d.	n.d.	n.d.						x	x	
Alanine		x		x			x					x		
Asparagine								x				x		
Aspartic acid		x									x	x	x	x
Citric acid												x		
Fructose														
Fumaric acid														
Galactinol		x		x			x	x			x	x	x	x
Gluconic acid														
Glucose														
Glutamic acid		x									x			x
Glutamine		x									x			
Glycine														
Isoleucine				x							x			
Leucine				x							x			
Lysine		x		x							x			
Malic acid														
Melibiose														
Methionine	x										x			
Ornithine	x	x									x	x	x	x
Oxaloacetate	n.d.	n.d.	n.d.	n.d.	n.d.	n.d.								n.d.
Phenylalanine											x	x		
Proline							x	x	x	x	x	x	x	x
Putrescine	x	x		x					x	x	x			x
Pyruvic acid														
Raffinose													x	
Serine							x		x		x	x	x	x
Spermidine	x	x									x	x	x	
Succinic acid														
Sucrose				x							x		x	x
Threitol														
Threonic acid		x									x	x	x	x
Threonine							x		x		x			x
Tryptophan									x					
Tyrosine		x												
Valine				x			x		x					
myo-Inositol		x									x		x	x
Maltose		x		x			x	x	x		x		x	x

are two possible explanations for this finding: either the higher maximum quantum yield in *gin2-1* indeed proves better integrity of PSII, which is unexpected given its HL sensitivity, or *gin2-1* failed to respond to the stress condition. A sustained reduction of maximum quantum yield can effectuate protection against oxidative stress (Adams III *et al.*, 2008), and thus keeping a high F_V/F_M at high irradiance could in fact be counter-productive. Sensitivity of *gin2-1* to HL stress became visible as a reduction in photochemical quenching (qP) and actual quantum yield (qY) under HL (Figure 2c). Although differences between *Ler*

and *gin2-1* were not massive, their persistence over the entire light phase points to their contribution to growth difference between the two genotypes at increasing photon flux intensity.

HL sensitivity of *gin2-1* became obvious as a massive decline in proteins of PSII, PSI and the ATP producing redox chain (Figure S2e,f). A possible reason for the failure of *gin2-1* to adequately respond to high irradiance could be its inability to sense rising glucose concentrations, which in the wild type cause repression of photosynthetic genes (Cho *et al.*, 2006; Zhang *et al.*, 2008). Alternatively,

anthocyanin production could be hampered. Hu *et al.* (2016) demonstrated that in callus of *Malus domestica*, HXK1 modulates anthocyanin accumulation, indicating a role for HXK1 in photoprotection. The strong reduction in photosynthetic proteins in *gin2-1* (Figure S2e,f) may thus reflect protein degradation induced by oxidative damage of the photosystems (Aro *et al.*, 1993; Sharma *et al.*, 2011). Accordingly, massive damage also occurred in the ATP producing electron transport chain (ETC) in *gin2-1* already after 4 h in the HL (Figure S4e). This supports the concept that hexokinase plays an important role in provision of ADP in order to prevent accumulation of electrons in the ETC (Hatefi, 1985; Laterveer *et al.*, 1997).

Further support for the hypothesis of low responsiveness of *gin2-1* to elevated light availability comes from the finding that in comparison with *gin2-1* the wild type had elevated levels of enzymes belonging to amino acid synthesis after 4 h HL, while after 10 h enzymes participating in the TCA cycle and in the sugar/starch metabolism were more abundant than in *gin2-1* (Figure S2a,b). Both findings indicate increased metabolite processing in *Ler* in response to elevated photosynthetic activity, while *gin2-1* failed to respond. To analyze how this differential response to HL stress transduced into metabolism, a compartmentalized metabolomics approach was employed that, in combination with compartment-specific protein analysis, achieved a much higher resolution than in previous studies (Hoermiller *et al.*, 2017).

Subcellular metabolomics of stress responses

Under HL, increased levels of glucose, fructose, amino acids and organic acids were found, indicating either increased photosynthetic activity, or decreased assimilate export. In the case of glycine, an increased rate of photorespiration or a reduced mitochondrial glycine decarboxylase activity under HL could be the cause. Similar results have been reported by Wulff-Zottele *et al.* (2010) who applied HL for six consecutive days. In this study, several metabolites, of which raffinose was representative, increased at day 1, then decreased at day 2 and again increased from day 3 to day 6. In the present work, raffinose showed a similar behaviour: after 4 h of HL exposition: the trisaccharide strongly increased in *Ler* and *gin2-1*, but then decreased in *Ler* after 10 h, while it further increased in *gin2-1* (Figure 8). Wulff-Zottele *et al.* (2010) described these oscillations as a fast response to a perturbation directed at re-adjustment to the initial metabolic state, before establishing a new homeostasis at the higher light intensity. This again would imply a faster response of *Ler* to the HL stress, while *gin2-1*, after 10 h, was still in the phase of massive perturbation of metabolite pools because of increased carbon assimilation. At a subcellular level, additional metabolite distributions, which supported a faster response in *Ler* compared with *gin2-1* were found, the most prominent being proline and serine.

Proline is known to acquire various protective functions under stress conditions, and therefore high proline concentrations in plants are frequently reported after stress exposure (Kaur and Asthir, 2015). Besides its role as an osmoprotectant (Hare *et al.*, 1998; Szabados and Savoure, 2010) proline synthesis might contribute to redox stabilization in supplying the chloroplasts with NADP⁺ as an electron acceptor, when Calvin–Benson cycle activity is insufficient to consume NADPH supplied by the ETC. It was shown by Székely *et al.* (2008) that mutants deficient in pyrroline-5-carboxylate synthase-1, having lower proline content, showed reduced activity of the ascorbate-glutathione cycle, which is an important ROS scavenging pathway (Foyer and Noctor, 2011; Noshi *et al.*, 2016). The higher proline content in *Ler* together with its faster association with the chloroplasts constitutes a clear advantage of the wildtype and may, at least in part, explain the light sensitive phenotype of *gin2-1*.

Although the total content of serine did not increase in either HL or cold treatments, its association with chloroplasts and mitochondria under HL was again faster in *Ler* than in *gin2-1*, similar to the observation for proline. Association of serine with mitochondria in HL is an indicator of elevated photorespiration that involves a shuttle of serine between mitochondria and peroxisomes. This is further supported by an increase in the total glycine concentration that is primarily depending on photorespiratory activity (Sicher and Barnaby, 2012). Photorespiration is widely accepted to fulfill a protective function in the cell as high energy consuming pathway that helps to prevent overreduction of the photosynthetic apparatus (Foyer *et al.*, 2009; Voss *et al.*, 2013).

Interestingly, under HL maltose was strongly associated with the plastids in *Ler* but not in *gin2-1*. Assuming constitutive activity of the maltose transporter MEX1 (Niittyä *et al.*, 2004), this would indicate current starch breakdown in *Ler* under HL. Evidence has been obtained for a redox regulation of starch degradation via the glucan-water dikinase GWD that phosphorylates starch (Lu and Sharkey, 2006) and the starch-degrading enzymes BAM1 and AMY3 (Santelia *et al.*, 2015). Considering the fast change of the oxidation state of roGFP under HL found in the current study, starch degradation could have been triggered by HL stress in *Ler* but not *gin2-1*. In contrast, both showed plastidial maltose in the cold. Maltose was reported to function as a protectant of the ETC under temperature stress (Kaplan and Guy, 2004; Lu and Sharkey, 2006). Studies investigating the protective behaviour of maltose have been carried out at a whole cell basis. Here it is shown that although maltose was in general higher in the *gin2-1* mutant, a distinct subcellular distribution for both genotypes was found at least under high irradiation. Especially during the first hours of stress, this might constitute a clear advantage of *Ler* over *gin2-1*.

For cold treated *Ler* and *gin2-1* plants an increase in fructose, glucose and sucrose within the first 10 h of stress treatment was observed as described earlier (Strand *et al.*, 1997; Kaplan *et al.*, 2007). While sucrose concentration increased two- to three-fold after 4 h and remained stable at 10 h of cold treatment, fructose and glucose further rose to levels 8- to 18-fold higher after 10 h in the cold (see Table 1). The 20- to 30-fold increase for fructose and glucose after 10 h described by Kaplan *et al.* (2007) may relate to a lower age of the plants or higher light intensity used in their study. Soluble sugars are described as protective agents due to their function as compatible solutes, protecting proteins and membranes from cold-induced damage (Wanner and Junttila, 1999; Uemura and Steponkus, 2003; Hannah *et al.*, 2006). While raffinose, as well as proline, showed high variability in control samples, higher values of proline and raffinose were found in *Ler* compared to *gin2-1* in the cold. Raffinose plays an important role in freezing tolerance (Korn *et al.*, 2010). It was shown by Hoermiller *et al.* (2017) that re-allocation of raffinose from the cytosol to the chloroplasts is firmly linked with the cold acclimation process. As there was no difference in the cold triggered subcellular re-distribution of raffinose in *Ler* and *gin2-1*, the delay found in the stress response of *gin2-1* under HL does not seem to occur in cold. In contrast, raffinose did accumulate already after 4 h in chloroplasts of HL treated *Ler* plants, while this took 10 h in *gin2-1* (Figure 8).

Although it must be emphasized that interpretation of metabolite association with mitochondria affords great care, because separation from the cytosol and chloroplasts is still not optimal, myo-inositol (MI) might be an interesting candidate for a protective agent in this compartment. MI and its derivatives are, in many species from bacteria to higher plants, correlated with tolerance to drought and/or salinity due to their role as osmolytes (Bohnert *et al.*, 1995). Here MI were associated with the chloroplasts under all conditions. However, under HL MI was also associated with the mitochondria, and this association was faster in *Ler* than in *gin2-1*. If indeed MI fulfills a role in protecting mitochondria from oxidative damage, the slow association with mitochondria could contribute to the light sensitivity of *gin2-1*. It has been demonstrated that MI interacts with HXK1 (Bruggeman *et al.*, 2015), and HXK1 is associated with mitochondrial membranes, probably involved in delivering substrates for glycolysis (Kim *et al.*, 2013).

CONCLUSION

The role of HXK1 in abiotic stress tolerance is under debate, and contradictory findings in the literature underline the complex and difficult interaction between sugar signalling and stress tolerance. Here it is shown that the subcellular distribution of metabolites is highly significant for judging possible roles in stress tolerance and acclimation. Results obtained for roGFP2 expressing transgenic

lines, as well as ChIF measurements, proteomics and sub-cellular metabolite analysis in *Ler* and its HXK1 deficient mutant, *gin2-1*, bear strong evidence that the *gin2-1* mutant appears slower in responding to HL stress, thus leading to an irradiance-dependent impairment of growth. In contrast, responses were not delayed for a cold treatment, even though both genotypes generally reacted differently to the two abiotic stress conditions.

EXPERIMENTAL PROCEDURES

Plant material and growth conditions

Arabidopsis thaliana (L.) Heynh. accession Landsberg *erecta* (*Ler*) and the *gin2-1* T-DNA insertion line of hexokinase 1 (At4g29130), Col-0 and roGFP2 plants, were grown in a 1:1 mixture of GS90 soil and vermiculite in a growth chamber with a 8 h/16 h light/dark regime ($120 \mu\text{mol m}^{-2} \text{sec}^{-1}$; $22^\circ\text{C}/16^\circ\text{C}$; 70% relative air humidity). As a standard procedure, plants were transferred to long-day condition after 5 weeks with a 16 h/8 h light/dark rhythm to obtain higher biomass. Plants were watered regularly and fertilized with standard nitrogen-phosphate-potassium fertilizer immediately after pricking, 10 days before and 4 days after transfer to long-day condition. Eight days after transfer to long-day condition, before the plants started flowering, *Ler* and *gin2-1* were harvested at three time points: (i) immediately before the light turned on ('08 h'); (ii) after 4 h ('12 h'); and (iii) after 10 h in the light ('18 h'). Hence, on harvest day two treatments and the control condition were sampled: (i) control condition (RT, $120 \mu\text{mol m}^{-2} \text{sec}^{-1}$); (ii) HL condition ($1100\text{--}1500 \mu\text{mol m}^{-2} \text{sec}^{-1}$, max. 30°C); and (iii) cold condition (4°C , $120 \mu\text{mol m}^{-2} \text{sec}^{-1}$). For *gin2-1* two rosettes were pooled for one independent sample. Samples were immediately frozen in liquid nitrogen, frozen leaves were ground to a fine powder using a MM200 ball mill (Retsch GmbH, www.retsch.de) and stored at -80°C until further use.

Analysis of roGFP2 plants

Four *Arabidopsis* lines expressing a reduction–oxidation-sensitive green fluorescent protein 2 (roGFP2; Schwarzländer *et al.*, 2016) were provided by Prof. Dr. Markus Schwarzländer (University of Münster, Germany). The expression of roGFP2 was compartment specific in each line for mitochondria, chloroplast, peroxisomes or the cytosol. The roGFP plants were grown in 1:1 mixture of GS90 soil and vermiculite as described above: 5 weeks in a growth chamber with a 8 h/16 h light/dark regime ($120 \mu\text{mol m}^{-2} \text{sec}^{-1}$; $22^\circ\text{C}/16^\circ\text{C}$; 70% relative air humidity), after 5 weeks the plants were transferred to long-day condition with a 16 h/8 h light/dark rhythm. After 8 days under long-day conditions the plants were analyzed either under control or HL conditions ($1100\text{--}1500 \mu\text{mol m}^{-2} \text{sec}^{-1}$, max. 30°C). Analysis of roGFP2 fluorescence was carried out as described in Rosenwasser *et al.* (2010) with a 96-well plate reader (TECAN-SpectraFluor Plus, Männedorf, Switzerland). Shortly, leaf discs were cut out and immediately floated on $200 \mu\text{l}$ distilled water. Fluorescence measurements were performed using 528 nm emission and 400 nm excitation. The leaf discs were further treated with 50 mM H_2O_2 to investigate fully oxidized roGFP. Subsequently, the leaf discs were washed and transferred to 50 mM DTT to measure fully reduced roGFP. Leaf discs were always floated with their ad-axial side up. OxD and the redox potential were calculated as described (Schwarzländer *et al.*, 2008). Midpoint potential for roGFP2 was considered to be -272 mV (Hanson *et al.*, 2004) and

compartment-specific pH values were assumed to be: 7.2 for the cytoplasm, 7.8 for mitochondria, 8.0 for plastids and 8.3 for peroxisomes (Shen *et al.*, 2013).

Chlorophyll fluorescence

Chlorophyll fluorescence was determined by a Handy FluorCam (Photon Systems Instruments, Brno, Czech Republic, www.psi.cz). The instrument was operated according to the manufacturer's instruction with slight modifications. Briefly, a protocol of 250 sec was used to capture time-resolved ChlF images from plant rosettes. The protocol started with measurement of basal fluorescence (F_0) and maximum fluorescence (F_M) by using measuring and saturating flashes. After a short dark period (20 sec), actinic light of $120 \mu\text{mol m}^{-2} \text{sec}^{-1}$ (or $1200 \mu\text{mol m}^{-2} \text{sec}^{-1}$ for HL plants) was applied and fluorescence transients were determined. Seven strong flashes of saturating light every 25 sec were overlaid with actinic light to investigate activation of non-photochemical quenching. Seven to 10 individual plants per genotype and condition were analyzed. The images of the ChlF transients were averaged across the rosettes for quantitative evaluation of fluorescence parameters.

Non-aqueous fractionation

Non-aqueous fractionation was performed as described earlier (Nägele and Heyer, 2013; Hoermiller *et al.*, 2017). Shortly, 100–150 mg freeze-dried plant homogenate were suspended in 10 ml heptane-tetrachloroethylene ($\rho = 1.3 \text{ g ml}^{-1}$). The suspension was sonified on ice for 12 min with repeated intervals of 5 sec pulse and 15 sec pause (Branson Sonifier 250, Branson, USA). The sonified suspension was diluted with 10 ml heptane, filtered through a $30 \mu\text{m}$ nylon gauze and centrifuged at 4°C for 10 min at 2350 g. The sediment was resuspended in 1 ml heptane-tetrachloroethylene ($\rho = 1.3 \text{ g ml}^{-1}$) and loaded on a linear gradient of heptane-tetrachloroethylene ($\rho = 1.3 \text{ g ml}^{-1}$) to pure tetrachloroethylene ($\rho = 1.6 \text{ g ml}^{-1}$). After ultracentrifugation at 100 000 g for 3 h 30 min at 4°C the gradient was separated into nine fractions of equal volume. These fractions were further aliquoted into subfractions of equal volume, dried under vacuum and the activity of marker enzymes were determined as described earlier (Knaupp *et al.*, 2011; Nägele and Heyer, 2013): alkaline pyrophosphatase as plastidial marker, UGPase as cytosolic marker and acid phosphatase as vacuolar marker. Sub-fractions were further used for proteome and metabolome analysis on liquid and gas chromatography coupled to mass spectrometry (LC-MS/MS and GC-MS ToF respectively).

Extraction and protein analysis via LC-MS/MS

Dried pellets from fractionated gradients were solubilized in 8 M urea, 50 mM Hepes KOH (pH = 7.8) on ice. Samples were precipitated in acetone with 0.5% beta-mercaptoethanol. Pellets were washed two times with methanol and acetone, and afterwards again solubilized in 8 M urea, 50 mM Hepes KOH (pH = 7.8). Protein concentration was determined via the Bio-Rad Bradford-assay using BSA as the standard. Equal amounts of protein (15 μg) were reduced with dithiothreitol (DTT) at a concentration of 5 mM for 45 min at 37°C , and alkylated at a concentration of 10 mM with iodoacetamide (IAA) and incubated dark for 60 min at 23°C . Alkylation was stopped by increasing DTT concentration to 10 mM and dark incubated for 15 min. Samples were two-fold diluted by 20% acetonitrile (ACN) and 100 mM ammonium bicarbonate (AmBic), proteins were pre-digested with Lys-C (1:1000 w:w; Sigma-Aldrich) at 30°C for 2.5 h dark. Samples were two-fold diluted to 2 M urea by 10% ACN, 25 mM AmBic, 10 mM CaCl_2 and

digested with sequencing grade modified trypsin (Poroszyme, immobilized trypsin; 1:100 v:w) for 12 h. Digested proteins were acidified with formic acid (pH \sim 3.0) and desalted with C18 materials (Agilent, Bond Elut SPEC) and dried in a vacuum concentrator (ScanVac, LaboGene). Peptides were solved in 2% ACN, 0.1% formic acid and the same amounts of total protein were loaded and separated on a PepMap RSLC $75 \mu\text{m}$, 50 cm column (Thermo Fisher Scientific Inc., Waltham, USA). The flow rate was set to 300 nl min^{-1} with 2–40% in 90 min of mobile phase B (mobile phase A: 0.1% formic acid (FA) in water (v/v); mobile phase B: 0.1% FA in 90% ACN (v/v)) and further from 40 to 90% in 1 min and stable at 90% for 5 min, with 53 min of equilibration phase at the end. MS analysis was performed with an Orbitrap Elite instrument (Thermo Fisher Scientific Inc., Waltham, USA) in positive mode and full scan in FT with a resolution of 60 000 in profile mode. Precursor masses ranged at 360–1800 m/z, and MS/MS rapid centroid mode in the linear ion trap with CID fragmentation for the 20 most intense ions, by a minimal signal threshold of 500 counts. Prediction of ion injection time was enabled (5×10^2 ions for up to 10 msec). Dynamic exclusion was enabled with repeat count 1 and repeat duration of 30 sec; exclusion list size was set to 500 and exclusion duration for 30 sec. Excluded mass was set to ± 10 ppm relative to reference mass, early expiration enabled with 1 count and s/n threshold of 2.0. Activation was CID, with a default charge state of 2, isolation width at 2.0 m/z, normalized collision energy at 35.0, activation q at 0.250 and an activation time of 10.00 msec.

Peptide identification as well as protein quantification were performed using the software Maxquant (<http://www.maxquant.org>) and implemented algorithms of version 1.5.5.1 (Cox and Mann, 2008) against the TAIR10 (www.arabidopsis.org) protein database (Lamesch *et al.*, 2012). Protein analysis for label-free quantification was done with main settings as recommended. Shortly, maximum two missed cleavages were used, variable modifications with maximal five numbers of modifications per peptide were allowed for N-terminal acetylation and methionine oxidation and as fixed a modification carbamidomethylation was set. For identification, a minimum of two peptides and two minimum razor + unique peptides were requested. Maxquant LFQ protein output was normalized to total protein amount per fraction. Whole gradients were additionally normalized to inserted dry weight. Further details about subcellular markers can be found in the accompanying article (Fürtauer *et al.*, 2019).

Extraction and analysis of primary metabolites by GC-MS ToF

Primary metabolite concentrations were quantified with gas chromatography coupled to time-of-flight mass spectrometry. Non-fractionated and fractionated gradients were extracted as published previously (Weiszmann *et al.*, 2017). Shortly, samples were extracted twice on ice with methanol:chloroform:water (MCW, 5:2:1 v:v:v), followed by an extraction step with 80% ethanol in which the pellets were heated up to 80°C for 30 min. For phase separation, water was added to the MCW supernatant and the polar phase was merged with the ethanol extract and dried in a vacuum concentrator (ScanVac, LaboGene). The dried extracts were derivatized applying methoximation (methoxyamine hydrochloride in pyridine) by incubation for 90 min at 30°C . For silylation, N-methyl-N-(trimethylsilyl) trifluoroacetamide was used and samples were incubated for 30 min at 37°C . Derivatized samples were transferred into glass vials, which were sealed with a crimp cap. GC-ToF-MS analysis was performed on an Agilent 6890 gas chromatograph (Agilent Technologies®, Santa Clara,

USA) coupled to a LECO Pegasus® GCxGC–TOF mass spectrometer (LECO Corporation, St. Joseph, USA). Compounds were separated on an Agilent column HP5MS (length: 30 m, diameter: 0.25 mm, film: 0.25 µm). Deconvolution of the total ion chromatogram and peak integration was performed using the software LECO Chromatof®. For each metabolite, calibration curves were recorded. Within gradients, relative distribution of metabolites was determined. For absolute quantification, dried non-fractionated plant material was extracted as described above, and calibration curves of six different concentrations within the linear range of detection were used.

Determination of subcellular metabolite distributions

Subcellular metabolite distribution of each fractionated sample was calculated as described previously (Fürtauer *et al.*, 2016). The algorithm applied compares distribution of marker proteins and metabolites between all subfractions of one sample. To prevent overestimation of technical errors introduced by LC-MS/MS and GC-MS quantification of proteins and metabolites, only those subcellular fractions were correlated which differed $\geq 10\%$ in their marker protein levels and $\geq 5\%$ in metabolite levels. Absolute subcellular metabolite levels were calculated by multiplication of each relative distribution with the absolute concentration that was determined from non-fractionated plant material (see Fürtauer *et al.*, 2019, for further detail).

Data analysis and statistics

Data evaluation, normalization and visualization were performed in Microsoft Excel® (<http://www.microsoft.com>) and the numerical software Matlab (version R2014a; The Mathworks Inc, MA, USA). Analysis of variance, Tukey's Honestly Significant Difference (HSD) test and Student's t-test were performed with the R software (R Core Team, 2016; The R Project for Statistical Computing; <http://www.r-project.org/>), comparisons were considered to be significant for P -values < 0.05 . Assignment and categorization of proteins were done using the MapMan tool, version 3.6.0 RC1 with ontology version Ath_AGI_TAIR9_Jan2010.m02. Venn diagrams were created using the online tool Venny 2.1.0 (Oliveros, 2007–2015).

DATA STATEMENT

All data generated and used in this study are available upon request or as Supporting Information of the article.

ACKNOWLEDGEMENTS

This research was funded by the German Science Foundation (DFG) through grant HE3087/11-1 and the Austrian Science Fund (FWF) Project I 2071. We thank Prof. Dr. Markus Schwarzländer, University of Münster (Germany) for providing roGFP2 seeds. We would like to thank members of the Dept. Plant Biotechnology (University Stuttgart), Dept. Ecogenomics and Systems Biology (University of Vienna) and Dept. Biology I (LMU Munich) for fruitful discussions and constructive advice. We thank Diether Gotthardt, Marvin Müller and Annika Allinger for excellent plant cultivation and Martin Brenner for technical assistance.

CONFLICT OF INTEREST

The authors declare no conflict of interest.

AUTHOR CONTRIBUTIONS

LK and LF performed experiments, data evaluation and wrote the manuscript. WW supported metabolomics and

proteomics analysis. TN and AGH conceived the study, performed data evaluation and wrote the manuscript.

SUPPORTING INFORMATION

Additional Supporting Information may be found in the online version of this article.

Figure S1. Principal component analysis (PCA) of metabolite distribution after 4 h in cold or high light condition.

Figure S2. MapMan analysis of significantly different abundant proteins of high light treatment.

Figure S3. MapMan analysis of significantly different abundant proteins of cold treatment.

Figure S4. MapMan analysis of significantly different abundant proteins, focused on the photosynthetic machinery, of the high light treatment.

Table S1. Mean ratios of chlorophyll fluorescence measurements for gin2-1 and Ler.

Table S2. Significantly changed proteins between normal and stress conditions (t-test, $P < 0.025$; Bonferroni corrected).

Table S3. Distribution of the measured metabolites in the three compartment model.

Table S4. Distribution of the measured metabolites in the four compartment model.

Table S5. Metabolite data for PCA analysis.

REFERENCES

- Alvarez, M.E., Pennell, R.I., Meijer, P.-J., Ishikawa, A., Dixon, R.A. and Lamb, C. (1998) Reactive oxygen intermediates mediate a systemic signal network in the establishment of plant immunity. *Cell*, **92**, 773–784.
- Aro, E.-M., Virgin, I. and Andersson, B. (1993) Photoinhibition of photosystem II. Inactivation, protein damage and turnover. *BBA-Bioenergetics*, **1143**, 113–134.
- Adams III, W.W., Zarter, C.R., Mueh, K.E., Amiard, V. and Demmig-Adams, B. (2008) Energy dissipation and photoinhibition: A continuum of photoprotection. In *Photoprotection, Photoinhibition, Gene Regulation, and Environment* (Demmig-Adams, B., Adams, W.W. and Mattoo, A.K., eds). Dordrecht, The Netherlands: Springer, pp. 49–64.
- Baxter, A., Mittler, R. and Suzuki, N. (2014) ROS as key players in plant stress signalling. *J. Exp. Bot.* **65**, 1229–1240.
- Björkman, O. and Demmig, B. (1987) Photon yield of O₂ evolution and chlorophyll fluorescence characteristics at 77 K among vascular plants of diverse origins. *Planta*, **170**, 489–504.
- Blokhina, O.B. (2001) Anoxic stress leads to hydrogen peroxide formation in plant cells. *J. Exp. Bot.* **52**, 1179–1190.
- Bohnert, H.J., Nelson, D.E. and Jensen, R.G. (1995) Adaptations to environmental stresses. *Plant Cell*, **7**, 1099–1111.
- Bolwell, G.P. and Wojtaszek, P. (1997) Mechanisms for the generation of reactive oxygen species in plant defence – a broad perspective. *Physiol. Mol. Plant Pathol.* **51**, 347–366.
- Brauner, K., Stutz, S., Paul, M. and Heyer, A.G. (2015) Measuring whole plant CO₂ exchange with the environment reveals opposing effects of the gin2-1 mutation in shoots and roots of Arabidopsis thaliana. *Plant Signal. Behav.* **10**, e973822.
- Bruggeman, Q., Prunier, F., Mazubert, C., de Bont, L., Garnier, M., Luga, R., Benhamed, M., Bergounioux, C., Raynaud, C. and Delarue, M. (2015) Involvement of Arabidopsis hexokinase1 in cell death mediated by Myo-inositol accumulation. *Plant Cell*, **27**, 1801–1814.
- Cho, Y.-H., Yoo, S.-D. and Sheen, J. (2006) Regulatory functions of nuclear hexokinase1 complex in glucose signaling. *Cell*, **127**, 579–589.
- Choudhury, F.K., Rivero, R.M., Blumwald, E. and Mittler, R. (2017) Reactive oxygen species, abiotic stress and stress combination. *Plant J.* **90**, 856–867.
- Cox, J. and Mann, M. (2008) MaxQuant enables high peptide identification rates, individualized p.p.b.-range mass accuracies and proteome-wide protein quantification. *Nat. Biotechnol.* **26**, 1367–1372.

- Dietz, K.-J. (2017) Subcellular metabolomics: the choice of method depends on the aim of the study. *J. Exp. Bot.* **68**, 5695–5698.
- Foyer, C.H. and Noctor, G. (2003) Redox sensing and signalling associated with reactive oxygen in chloroplasts, peroxisomes and mitochondria. *Physiol. Plant.* **119**, 355–364.
- Foyer, C.H. and Noctor, G. (2011) Ascorbate and glutathione. The heart of the redox hub. *Plant Physiol.* **155**, 2–18.
- Foyer, C.H. and Noctor, G. (2015) Defining robust redox signalling within the context of the plant cell. *Plant Cell Environ.* **38**, 239.
- Foyer, C.H., Lopez-Delgado, H., Dat, J.F. and Scott, I.M. (1997) Hydrogen peroxide- and glutathione-associated mechanisms of acclimatory stress tolerance and signalling. *Physiol. Plant.* **100**, 241–254.
- Foyer, C.H., Bloom, A.J., Queval, G. and Noctor, G. (2009) Photorespiratory metabolism. Genes, mutants, energetics, and redox signaling. *Annu. Rev. Plant Biol.* **60**, 455–484.
- Fürtauer, L., Weckwerth, W. and Nägele, T. (2016) A benchtop fractionation procedure for subcellular analysis of the plant metabolome. *Front. Plant Sci.* **7**, 1912.
- Fürtauer, L., Küstner, L., Weckwerth, W., Heyer, A. G. and Nägele T. (2019) Resolving subcellular plant metabolism. *Plant J.* <https://doi.org/10.1111/tbj.14472>
- Hannah, M.A., Wiese, D., Freund, S., Fiehn, O., Heyer, A.G. and Hinch, D.K. (2006) Natural genetic variation of freezing tolerance in Arabidopsis. *Plant Physiol.* **142**, 98–112.
- Hanson, G.T., Aggeler, R., Oglesbee, D., Cannon, M., Capaldi, R.A., Tsien, R.Y. and Remington, S.J. (2004) Investigating Mitochondrial Redox Potential with Redox-sensitive Green Fluorescent Protein Indicators. *J. Biol. Chem.* **279**, 13044–13053.
- Hare, P.D., Cress, W.A. and van Staden, J. (1998) Dissecting the roles of osmolyte accumulation during stress. *Plant Cell Environ.* **21**, 535–553.
- Harrington, G.N. and Bush, D.R. (2003) The bifunctional role of hexokinase in metabolism and glucose signaling. *Plant Cell*, **15**, 2493–2496.
- Hatefi, Y. (1985) The mitochondrial electron transport and oxidative phosphorylation system. *Ann. Rev. Biochem.* **54**, 1015–1069.
- Heyneke, E., Luschin-Ebengreuth, N., Krajcser, I., Wolkinger, V., Müller, M. and Zechmann, B. (2013) Dynamic compartment specific changes in glutathione and ascorbate levels in Arabidopsis plants exposed to different light intensities. *BMC Plant Biol.* **13**, 104.
- Hoermiller, I.I., Naegle, T., Augustin, H., Stutz, S., Weckwerth, W. and Heyer, A.G. (2017) Subcellular reprogramming of metabolism during cold acclimation in Arabidopsis thaliana. *Plant Cell Environ.* **40**, 602–610.
- Houshyani, B., Kabouw, P., Muth, D., de Vos, R.C.H., Bino, R.J. and Bouwmeester, H.J. (2012) Characterization of the natural variation in Arabidopsis thaliana metabolome by the analysis of metabolic distance. *Metabolomics*, **8**, 131–145.
- Hu, D.-G., Sun, C.-H., Zhang, Q.-Y., An, J.-P., You, C.-X. and Hao, Y.-J. (2016) Glucose sensor MdHXK1 phosphorylates and stabilizes MdbHLH3 to promote anthocyanin biosynthesis in apple. *PLoS Genet.* **12**, e1006273.
- Huber, S. (1989) Biochemical mechanism for regulation of sucrose accumulation in leaves during photosynthesis. *Plant Physiol.* **91**, 656–662.
- Jorge, T.F., Rodrigues, J.A., Caldana, C., Schmidt, R., van Dongen, J.T., Thomas-Oates, J. and António, C. (2016) Mass spectrometry-based plant metabolomics. Metabolite responses to abiotic stress. *Mass Spectrom. Rev.* **35**, 620–649.
- Kaplan, F. and Guy, C.L. (2004) beta-Amylase induction and the protective role of maltose during temperature shock. *Plant Physiol.* **135**, 1674–1684.
- Kaplan, F., Kopka, J., Sung, D.Y., Zhao, W., Popp, M., Porat, R. and Guy, C.L. (2007) Transcript and metabolite profiling during cold acclimation of Arabidopsis reveals an intricate relationship of cold-regulated gene expression with modifications in metabolite content. *Plant J.* **50**, 967–981.
- Karpinski, S. (1999) Systemic signaling and acclimation in response to excess excitation energy in Arabidopsis. *Science*, **284**, 654–657.
- Kaur, G. and Asthir, B. (2015) Proline. A key player in plant abiotic stress tolerance. *Biol. Plant.* **59**, 609–619.
- Kim, Y.-M., Heinzl, N., Giese, J.-O., Koeber, J., Melzer, M., Rutten, T., von Wirén, N., Sonnewald, U. and Hajirezaei, M.-R. (2013) A dual role of tobacco hexokinase 1 in primary metabolism and sugar sensing. *Plant Cell Environ.* **36**, 1311–1327.
- Knaupp, M., Mishra, K.B., Nedbal, L. and Heyer, A.G. (2011) Evidence for a role of raffinose in stabilizing photosystem II during freeze-thaw cycles. *Planta*, **234**, 477–486.
- Korn, M., Gärtner, T., Erban, A., Kopka, J., Selbig, J. and Hinch, D.K. (2010) Predicting Arabidopsis freezing tolerance and heterosis in freezing tolerance from metabolite composition. *Mol. Plant*, **3**, 224–235.
- Küstner, L., Nägele, T. and Heyer, A.G. (2019) Mathematical modeling of diurnal patterns of carbon allocation to shoot and root in Arabidopsis thaliana. *NPJ Syst. Biol. Appl.* **5**, 4.
- Lamesch, P., Berardini, T.Z., Li, D. et al. (2012) The Arabidopsis Information Resource (TAIR). Improved gene annotation and new tools. *Nucleic Acids Res.* **40**, D1202–D1210.
- Laterveer, F.D., Nicolay, K. and Gellerich, F.N. (1997) Experimental evidence for dynamic compartmentation of ADP at the mitochondrial periphery. Coupling of mitochondrial adenylate kinase and mitochondrial hexokinase with oxidative phosphorylation under conditions mimicking the intracellular colloid osmotic pressure. *Mol. Cell. Biochem.* **174**, 43–51.
- Lu, Y. and Sharkey, T.D. (2006) The importance of maltose in transitory starch breakdown. *Plant Cell Environ.* **29**, 353–366.
- Minocha, R., Majumdar, R. and Minocha, S.C. (2014) Polyamines and abiotic stress in plants. A complex relationship. *Front. Plant Sci.* **5**, 175.
- Mittler, R. (2002) Oxidative stress, antioxidants and stress tolerance. *Trends Plant Sci.* **7**, 405–410.
- Mittler, R. (2017) ROS are good. *Trends Plant Sci.* **22**, 11–19.
- Moore, B., Zhou, L., Rolland, F., Hall, Q., Cheng, W.-H., Liu, Y.-X., Hwang, I., Jones, T. and Sheen, J. (2003) Role of the Arabidopsis glucose sensor HXK1 in nutrient, light, and hormonal signaling. *Science*, **300**, 332–336.
- Nägele, T. and Heyer, A.G. (2013) Approximating subcellular organisation of carbohydrate metabolism during cold acclimation in different natural accessions of Arabidopsis thaliana. *New Phytol.* **198**, 777–787.
- Nägele, T., Henkel, S., Hörmiller, I., Sauter, T., Sawodny, O., Ederer, M. and Heyer, A. (2010) Mathematical modeling of the central carbohydrate metabolism in Arabidopsis reveals a substantial regulatory influence of vacuolar invertase on whole plant carbon metabolism. *Plant Physiol.* **153**, 260–272.
- Niittylä, T., Messerli, G., Trevisan, M., Chen, J., Smith, A.M. and Zeeman, S.C. (2004) A previously unknown maltose transporter essential for starch degradation in leaves. *Science*, **303**, 87–89.
- Noctor, G., Lelarge-Trouverie, C. and Mhamdi, A. (2015) The metabolomics of oxidative stress. *Phytochem.* **112**, 33–53.
- Noshi, M., Hatanaka, R., Tanabe, N., Terai, Y., Maruta, T. and Shigeoka, S. (2016) Redox regulation of ascorbate and glutathione by a chloroplastic dehydroascorbate reductase is required for high-light stress tolerance in Arabidopsis. *Biosci. Biotechnol. Biochem.* **80**, 870–877.
- Oliveros, J.C. (2007–2015) Venny. An interactive tool for comparing lists with Venn's diagrams. <http://bioinfo.cnb.csic.es/tools/venny/index.html>
- Orozco-Cárdenas, M.L., Narváez-Vásquez, J. and Ryan, C.A. (2001) Hydrogen peroxide acts as a second messenger for the induction of defense genes in tomato plants in response to wounding, systemin, and methyl jasmonate. *Plant Cell*, **13**, 179–191.
- Popova, A.V., Heyer, A.G. and Hinch, D.K. (2002) Differential destabilization of membranes by tryptophan and phenylalanine during freezing. The roles of lipid composition and membrane fusion. *BBA-Biomembranes*, **1561**, 109–118.
- Raghavendra, A.S., Reumann, S. and Heldt, H.W. (1998) Participation of mitochondrial metabolism in photorespiration. *Plant Physiol.* **116**, 1333–1337.
- Rolland, F., Baena-Gonzalez, E. and Sheen, J. (2006) Sugar sensing and signaling in plants: conserved and novel mechanisms. *Annu. Rev. Plant Biol.* **57**, 675–709.
- Rosenwasser, S., Rot, I., Meyer, A.J., Feldman, L., Jiang, K. and Friedman, H. (2010) A fluorometer-based method for monitoring oxidation of redox-sensitive GFP (roGFP) during development and extended dark stress. *Physiol. Plant.* **138**, 493–502.
- Santelia, D., Trost, P. and Sparla, F. (2015) New insights into redox control of starch degradation. *Curr. Opin. Plant Biol.* **25**, 1–9.
- Schneider, T. and Keller, F. (2009) Raffinose in chloroplasts is synthesized in the cytosol and transported across the chloroplast envelope. *Plant Cell Physiol.* **50**, 2174–2182.
- Schwarzländer, M., Dick, T.P., Meyer, A.J. and Morgan, B. (2016) Dissecting redox biology using fluorescent protein sensors. *Antioxid. Redox Signal.* **24**, 680–712.

- Schwarzländer, M., Fricker, M.D., Müller, C., Marty, L., Brach, T., Novak, J., Sweetlove, L.J., Hell, R. and Meyer, A.J. (2008) Confocal imaging of glutathione redox potential in living plant cells. *J. Microsc.* **231**, 299–316.
- Sharma, S., Villamor, J.G. and Verslues, P.E. (2011) Essential role of tissue-specific proline synthesis and catabolism in growth and redox balance at low water potential. *Plant Physiol.* **157**, 292–304.
- Shen, J., Zeng, Y., Zhuang, X., Sun, L., Yao, X., Pimpl, P. and Jiang, L. (2013) Organelle pH in the Arabidopsis Endomembrane System. *Mol. Plant*, **6**, 1419–1437.
- Sicher, R.C. (2011) Carbon partitioning and the impact of starch deficiency on the initial response of Arabidopsis to chilling temperatures. *Plant Sci.* **2011**, 167–176.
- Sicher, R.C. and Barnaby, J.Y. (2012) Impact of carbon dioxide enrichment on the responses of maize leaf transcripts and metabolites to water stress. *Physiol. Plant.* **144**, 238–253.
- Smeekens, S., Ma, J., Hanson, J. and Rolland, F. (2010) Sugar signals and molecular networks controlling plant growth. *Curr. Opin. Plant Biol.* **13**, 273–278.
- Strand, A., Hurry, V., Gustafsson, P. and Gardestrom, P. (1997) Development of Arabidopsis thaliana leaves at low temperatures releases the suppression of photosynthesis and photosynthetic gene expression despite the accumulation of soluble carbohydrates. *Plant J.* **12**, 605–614.
- Szabados, L. and Savoure, A. (2010) Proline: a multifunctional amino acid. *Trends Plant Sci.* **15**, 89–97.
- Székely, G., Abrahám, E., Cséplö, A. et al. (2008) Duplicated P5CS genes of Arabidopsis play distinct roles in stress regulation and developmental control of proline biosynthesis. *Plant J.* **53**, 11–28.
- Thimm, O., Bläsing, O., Gibon, Y., Nagel, A., Meyer, S., Krüger, P., Selbig, J., Müller, L.A., Rhee, S.Y. and Stitt, M. (2004) MapMan: a user-driven tool to display genomics data sets onto diagrams of metabolic pathways and other biological processes. *Plant J.* **37**, 914–939.
- Uemura, M. and Steponkus, P.L. (2003) Modification of the intracellular sugar content alters the incidence of freeze-induced membrane lesions of protoplasts isolated from Arabidopsis thaliana leaves. *Plant Cell Environ.* **26**, 1083–1096.
- Voss, I., Sunil, B., Scheibe, R. and Raghavendra, A.S. (2013) Emerging concept for the role of photorespiration as an important part of abiotic stress response. *Plant Biol.* **15**, 713–722.
- Wanner, L.A. and Juntila, O. (1999) Cold-induced freezing tolerance in Arabidopsis. *Plant Physiol.* **120**, 391–400.
- Weizmann, J., Fuertauer, L., Weckwerth, W. and Naegele, T. (2017) Vacuolar invertase activity shapes photosynthetic stress response of Arabidopsis thaliana and stabilizes central energy supply, *bioRxiv*, 168617
- Wulff-Zottele, C., Gatzke, N., Kopka, J., Orellana, A., Hoefgen, R., Fisahn, J. and Hesse, H. (2010) Photosynthesis and metabolism interact during acclimation of Arabidopsis thaliana to high irradiance and sulphur depletion. *Plant Cell Environ.* **33**, 1974–1988.
- You, J. and Chan, Z. (2015) ROS regulation during abiotic stress responses in crop plants. *Front. Plant Sci.* **6**, 1092.
- Yu, S., Cao, L., Zhou, C.-M., Zhang, T.-Q., Lian, H., Sun, Y., Wu, J., Huang, J., Wang, G. and Wang, J.-W. (2013) Sugar is an endogenous cue for juvenile-to-adult phase transition in plants. *eLife*, **2**, e00269.
- Zechmann, B. (2011) Subcellular distribution of ascorbate in plants. *Plant Signal. Behav.* **6**, 360–363.
- Zhang, H., Xie, X., Kim, M.-S., Korniyev, D.A., Holaday, S. and Paré, P.W. (2008) Soil bacteria augment Arabidopsis photosynthesis by decreasing glucose sensing and abscisic acid levels in planta. *Plant J.* **56**, 264–273.